LECTURE 7

[71] D.R.Hofstadter, Phys. Rev. B, v.14, 2239 (1976) [Harper model: electrons on a lattice in magnetic field].

[72] R.Lima, D.Shepelyansky, "Fast Delocalization in a Model of Quantum Kicked Rotator", Phys. Rev. Lett., v.67, N11, p.1377-1380 (1991) [delocalization of chaos in the kicked Harper model].

[73] T.Geisel, R.Ketzmerick and G.Petschel, Phys. Rev. Lett., v.67, p.3635 (1991); ibid, v.69, p.695 (1992) [kicked Harper model].

[74] R.Artuso, G.Casati, D.L.Shepelyansky, "Fractal Spectrum and Anomalous Diffusion in the Kicked Harper Model", Phys. Rev. Lett. v.68 N26 (1992) p.3826-3829.

[75] R.Artuso, F.Borgonovi, G.Casati, I.Guarneri and L.Rebuzzini, Int. J. Mod. Phys. B, v.8, p.207 (1994) [review on kicked Harper model].

[76] F.Borgonovi, D.L.Shepelyansky, "Spectral variety in the kicked Harper model", submitted to Europhys. Lett., July 1994 [indications on coexsistence of pure point, multi-fractal and continous spectrum in kicked Harper model].

[77] F.Benvenuto, G.Casati, I.Guarneri, D.L.Shepelyansky. "A Quantum Transition from Localized to Extended States in a Classically Chaotic System", Z.Phys.B - Condensed Matter, v.84, p.159 (1991) [delocalization transition in a triangular well model].

[78] D.L.Shepelyansky and A.D.Stone, Choatic Landau level mixing in classical and quantum wells, submitted to PRL (1994) [chaotic magneto-tunneling].

[79] G.Casati, I.Guarneri, D.L.Shepelyansky, "Anderson Transition in a One-Dimensional System with Three Incommensurate Frequencies", Phys. Rev. Lett. v.62, p.345-348 (1989).

[80] E.Ott, T.M.Antonsen Jr., J.D.Hanson, Phys. Rev. Lett., v.53, p.2187 (1984) [noise].

[81] D.Cohen, Phys. Rev. A, v.44, p.2292 (1991) [noise in quasimomentum].

[82] F.Borgonovi, D.L.Shepelyansky, "Adiabatic destruction of Anderson localization", Phys. Rev. E, (to be published) [adiabatic noise, slow parameter variation].

[83] E.Fermi, J.Pasta and S.Tsingou, Los Alamos preprint LA-1940 (1955); E.Fermi, Collected Papers, v.2, Univ. of Chikago Press, Chicago 1965, p.978 [FPU-problem].

[84] B.V.Chirikov and F.M.Izrailev, Sov. Phys. Dokl, v.11, N 1, p.30 (1966); B.V.Chirikov, F.M.Izrailev and V.A.Tayursky, Comput. Phys. Commun., v.5, p. 11 (1973) [chaos border in FPU-problem].

[85] J.Ford, Phys. Rep., v.213, p.271 (1992) [history of FPU-problem].

[86] H.Bauss, Newtonian casino, Penguin, 1990 (?) [how to win against roulette].
(title in USA: The Eudemonic Pie)
by Houghton Mifflin 1985

Kicked Harper model

$$\overline{\Psi} = U\Psi = \exp(-i\lambda)\,\Psi$$

$$U = \exp\left(-i\frac{L}{t}\cos(t\hat{n})\right)\exp\left(-i\frac{K}{t}\cos x\right)$$

$$\hat{n} = -i\frac{\partial}{\partial x}\,; \qquad \Psi(x+2\pi) = \Psi(x)\,; \qquad \hat{p} = t\hat{n}$$

Limit $\frac{L}{t}\,;\ \frac{K}{t} \to 0$ $\Rightarrow$ 2D electrons on a lattice in magnetic field (Harper, Azbel, Hofstadter, Thouless..

$$U = \exp(-iH/t)$$

Harper model

$$\begin{cases} H = L\cos\hat{p} + K\cos x \\ \mathcal{H} = H/L = \cos\hat{p} + \eta\cos x \end{cases}$$

$\frac{t}{2\pi} \Rightarrow \Phi/\Phi_0$ magnetic flux

$\hat{p} = t\hat{n} \qquad \eta = K/L$

$$\cos(tn)\,\Psi_n + \frac{\eta}{2}(\Psi_{n+1} + \Psi_{n-1}) = E\Psi_n$$

classical system is integrable

$\eta < 1$ exp. localized states

$\eta > 1$ delocalization (ballistic)

multifractal spectra

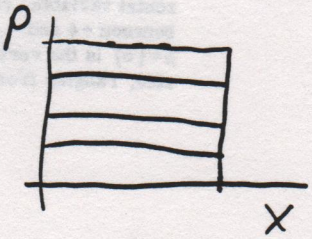

$\eta \ll 1$

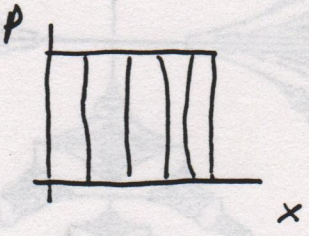

$\eta \gg 1$

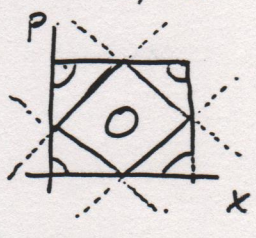

$K = L$

$\eta = 1$

q; hence one might expect the above condition to be satisfied in roughly q distinct regions of the ϵ axis (one region centered on each root). This is indeed the case, and is the basis for a very striking (and at first disturbing) fact about this problem: when $\alpha = p/q$, the Bloch band always breaks up into precisely q distinct energy bands. Since small variations in the magnitude of α can produce enormous fluctuations in the value of the denominator q, one is apparently faced with an unacceptable physical prediction. However, nature is ingenious enough to find a way out of this apparent anomaly. Before we go into the resolution, however, let us mention certain facts about the spectrum belonging to any value of α. Most can be proven trivially: (i) Spectrum(α) and spectrum ($\alpha + N$) are identical. (ii) Spectrum(α) and spectrum($-\alpha$) are identical. (iii) ϵ belongs to spectrum(α) if and only if $-\epsilon$ belongs to spectrum(α). (iv) If ϵ belongs to spectrum (α) for any α, then $-4 \leq \epsilon \leq +4$. The last property is a little subtler than the previous three; it can be proven in different ways. One proof has been published.[13]

From properties (i) and (iv), it follows that a graph of the spectrum need only include values of ϵ between +4 and −4, and values of α in any unit interval. We shall look at the interval $[0, 1]$. Furthermore, as a consequence of properties, the graph inside the above-defined rectangular region must have two axes of reflection, namely the horizontal line $\alpha = \frac{1}{2}$, and the vertical line $\epsilon = 0$. A plot of spectrum(α), with α along the vertical axis, appears in Fig. 1. (Only rational values of α with denominator less than 50 are shown.)

IV. RECURSIVE STRUCTURE OF THE GRAPH

This graph has some very unusual properties. The large gaps form a very striking pattern somewhat resembling a butterfly; perhaps equally striking are the delicacy and beauty of the fine-grained structure. These are due to a very intricate scheme, by which bands cluster into groups, which themselves may cluster into larger groups, and so on. The exact rules of formation of these hierarchically organized clustering patterns (Π's) are what we now wish to cover. Our description of Π's will be based on three statements, each of which describes some aspect of the structure of the graph. All of these statements are based on extremely close examination of the numerical data, and are to be taken as "empirically proven" theorems of mathematics. It would be preferable to have a rigorous proof but that has so far eluded capture. Before we present the three statements, let us first adopt some nomenclature. A "unit cell" is any portion of the graph located between successive integers N and $N+1$—in fact we will call that unit cell the Nth unit cell. Every unit cell has a "local variable" β, which runs from 0 to 1; in particular, β is defined to be the fractional part of α, usually denoted as $\{\alpha\}$. At $\beta = 0$ and $\beta = 1$, there is one band which stretches across the full width of the cell, separating it from its upper and lower neighbors; this band is therefore called a "cell wall." It turns out that certain rational values of β play a very important role in the description of the structure of a unit cell; these are the "pure cases"

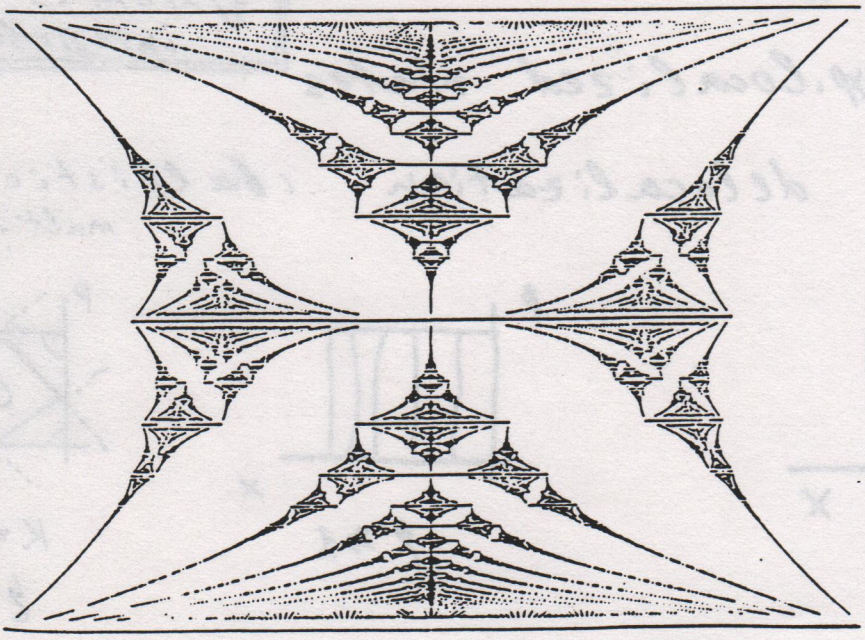

FIG. 1. Spectrum inside a unit cell. ϵ is the horizontal variable, ranging between +4 and −4, and $p = \{\alpha\}$ is the vertical variable, ranging from 0 to 1.

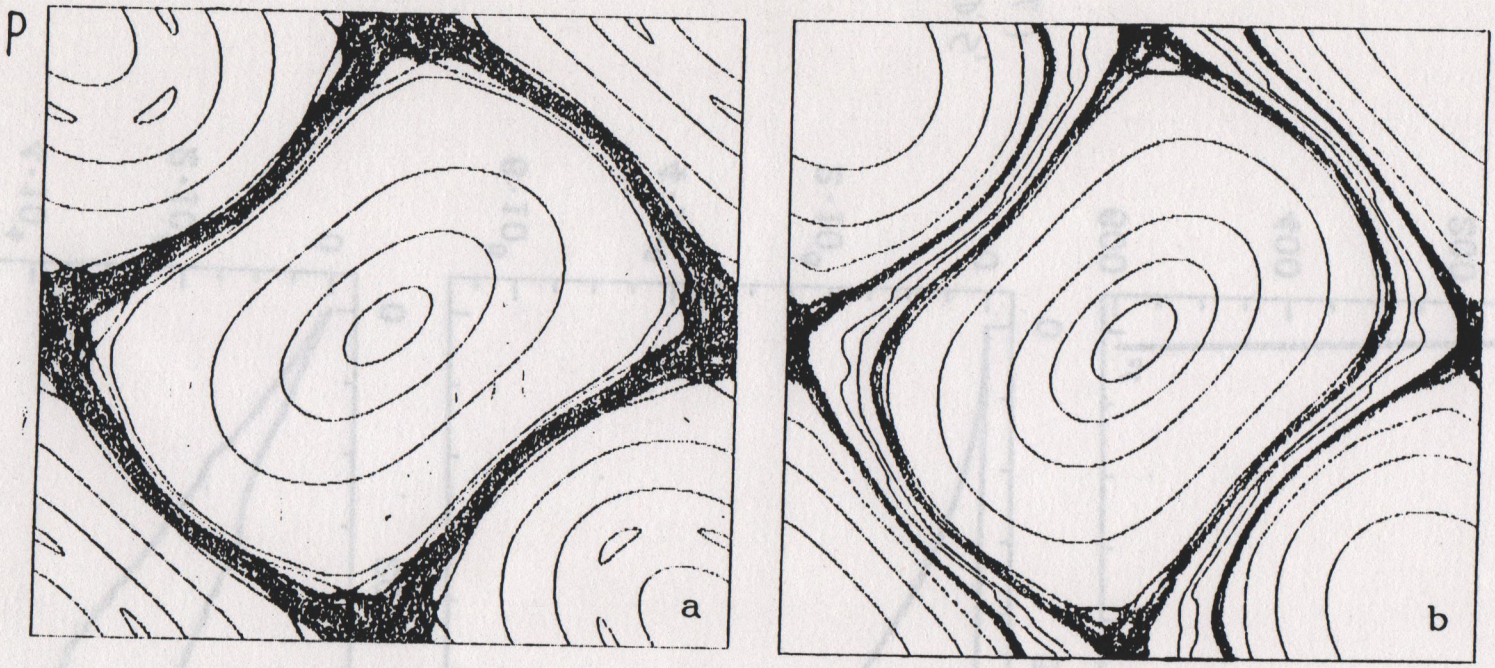

$K = L = 1.2$

$K = 1.2,\ L = 1$

$$\bar{p} = p + K \sin x$$

$$\bar{x} = x - L \sin \bar{p}$$

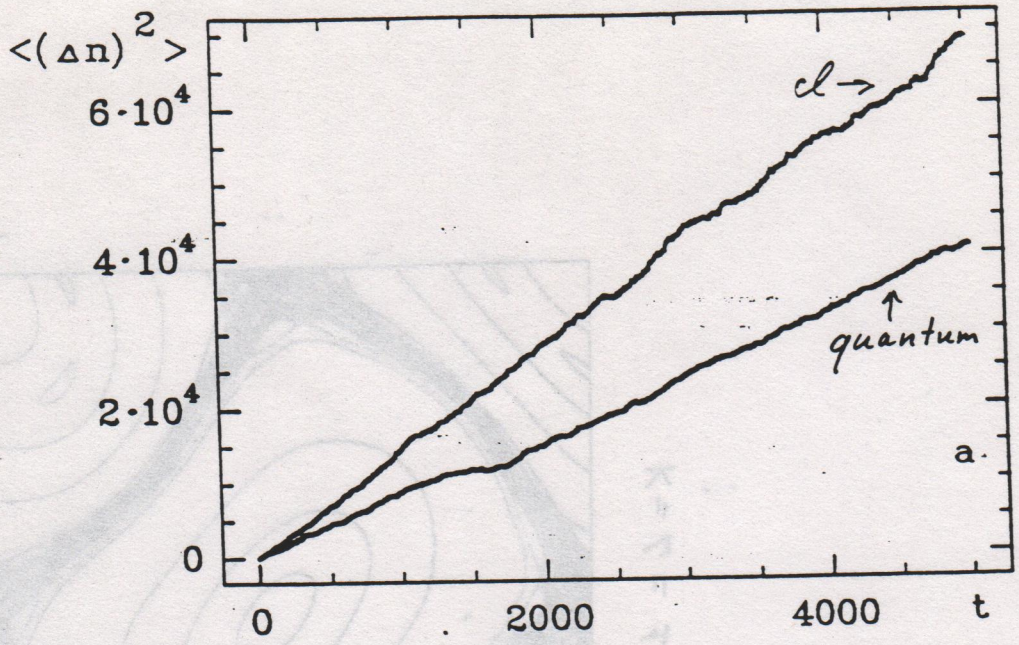

$K = L = 5$

$h = \frac{2\pi}{7.61803\ldots} \approx$

$\approx 0.824\ldots$

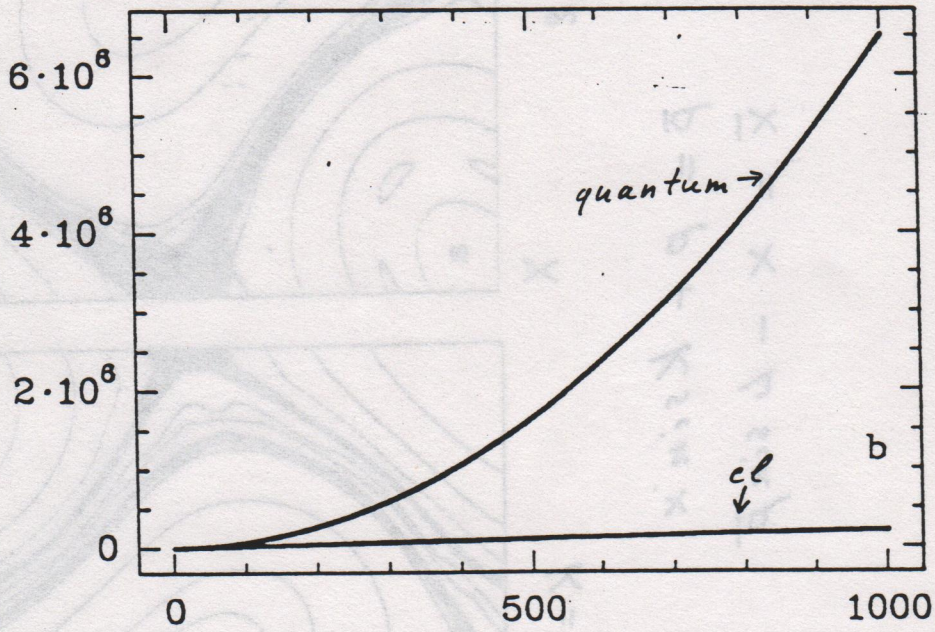

$K = 4,\ L = 2$

$h = \frac{2\pi}{25.61803\ldots} \approx$

$\approx 0.245\ldots$

ima, D.S.
(1991)

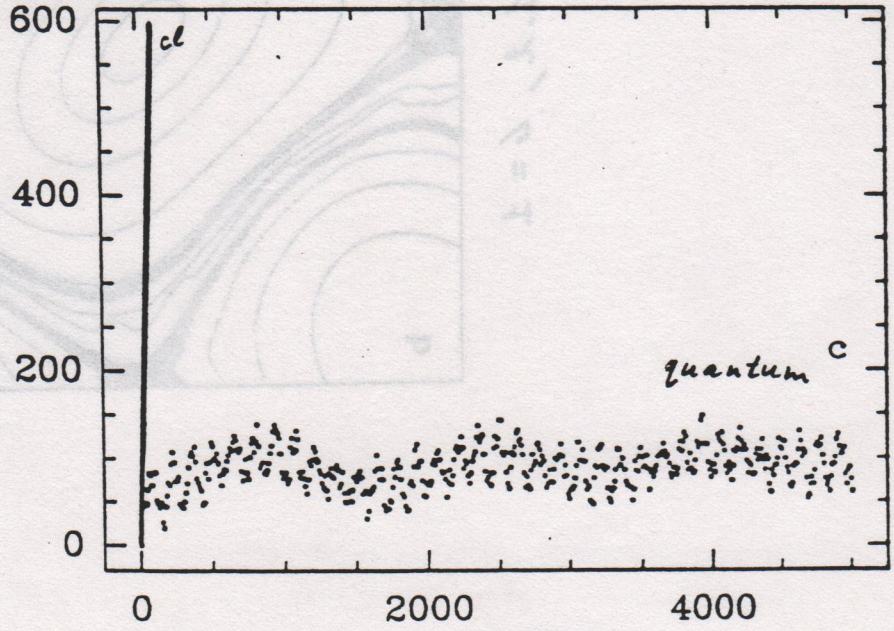

$K = 2,\ L = 4$

$h = \frac{2\pi}{25.61803\ldots} \approx$

$\approx 0.245\ldots$

(Lima, D.S.)
1991

Lima, D. S.
(1991)

$K = 4 = 5$

$\tau = \frac{2\pi}{7.61803\ldots} \simeq 0.824\ldots$

$t = 5000$

$n(t=0) = 0\,, \quad \beta = 0$

$K = 4$

λ

(Geisel et.al.)
(1992)

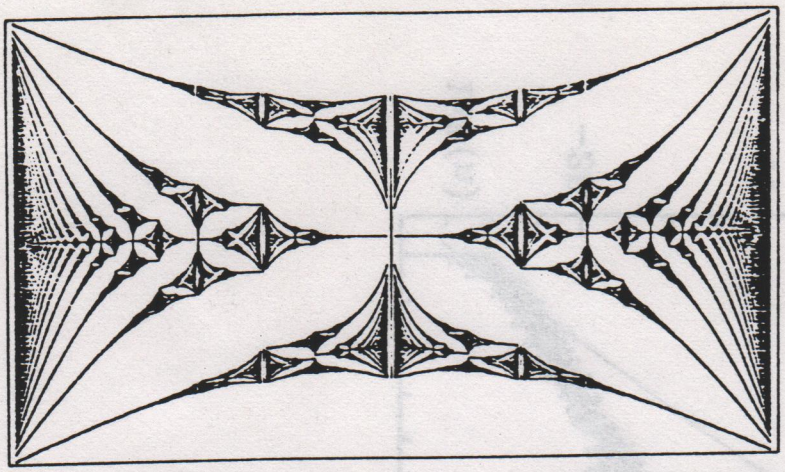

$\frac{K}{t} = 1$

$t/2\pi$

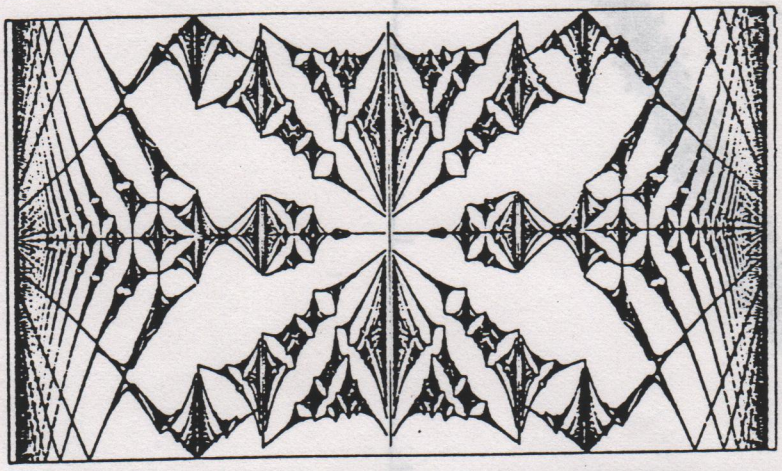

$\frac{K}{t} = 3$

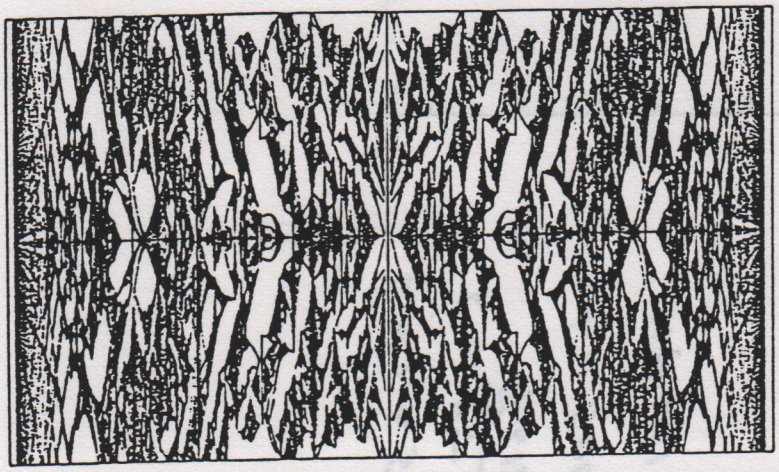

$\frac{K}{t} = 6$

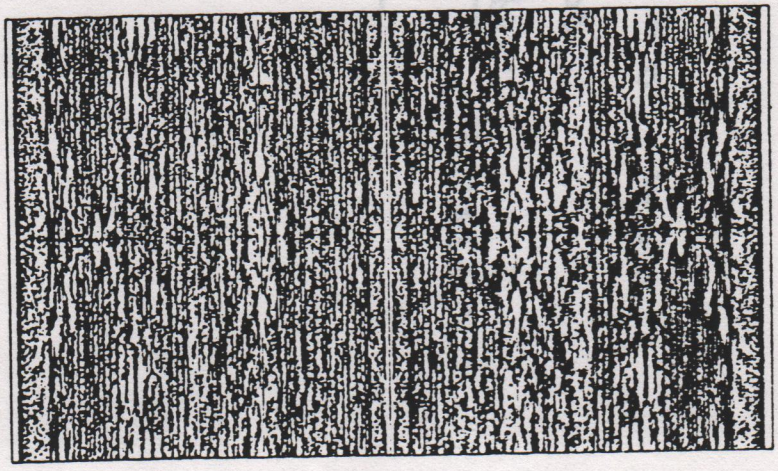

$\frac{K}{t} = 10$

Fig. 2

(Borgonovi, D. S. (1994)) Fig. 3

Inverse participation ration ξ in the kicked Harper model vs. quasienergy λ

$$U = \exp\left(-i \frac{L}{\hbar} \cos(\hbar n)\right) \exp\left(-i \frac{K}{\hbar} \cos x\right)$$

$K = 1$

$L = 7$

Localized phase

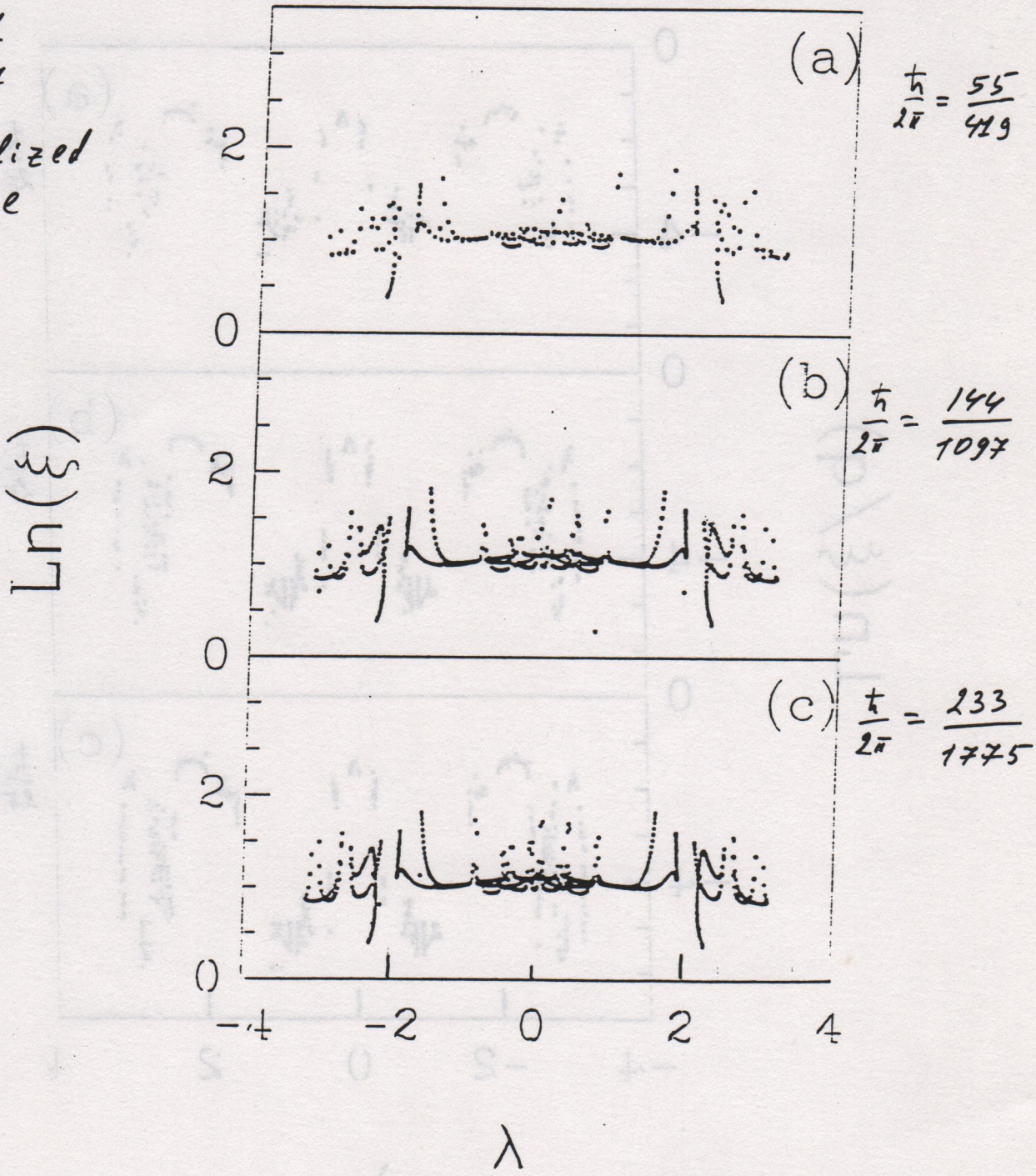

Borgonovi, D.S. (1994)

Fig. 4

the kicked Harper model

$K = 4, L = 7$ $\qquad \frac{h}{2\pi} = p/q$

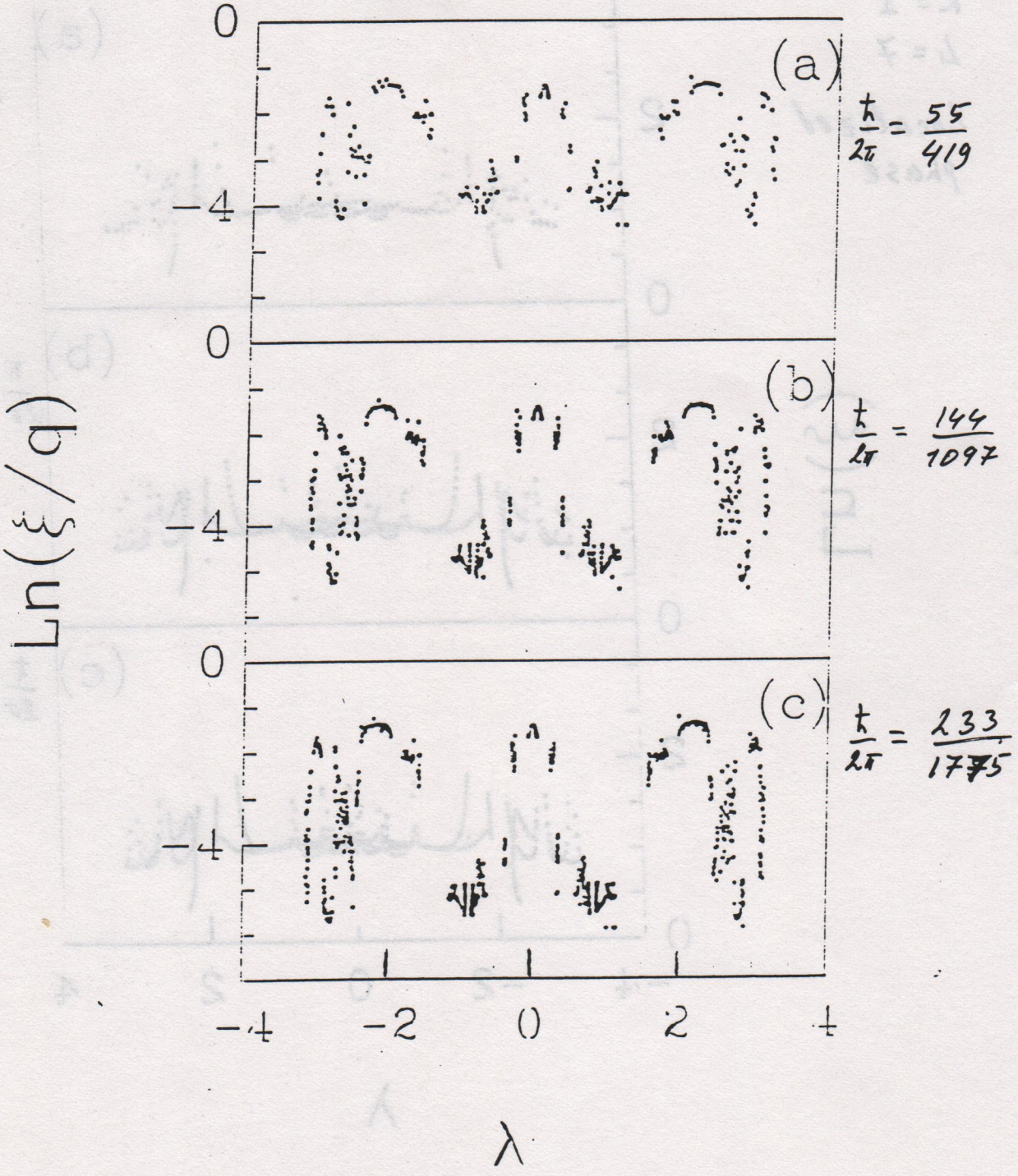

(56)

Kicked Harper model

$K, L \sim 4$ hard chaos

Effects of incommensurability in the domain of quantum chaos (Lima, D.S. (1991))

Delocalization transition

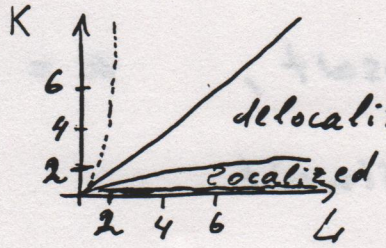

$\rightarrow$ { anomalouse diffusion $(\Delta n)^2 \sim t^\alpha$; $0 < \alpha < 2$
ballistic
$|\langle \Psi_0 | \Psi_t \rangle| \underset{t \to \infty}{\to}$ const

Quasi-energy spectrum is multifractal

clustering of levels

$\Delta V \sim \frac{1}{\Delta n}$ $\rightarrow$ is not a correct approximatio

$K = L$ - theorem about exsistence of delocalized states

Guarneri 1993

on the basis of reslults of Aubry, Bellissard

(Aubry duality $p \rightleftarrows x$)

(57)

Particle in a triangular well and a monochromatic field

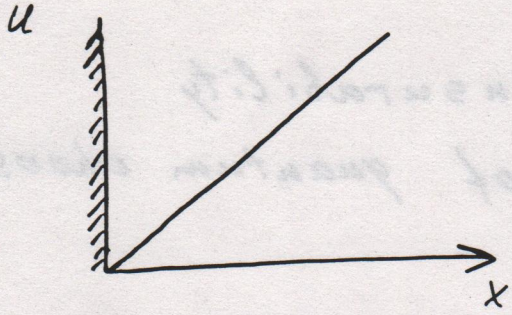

$$U = \varepsilon_0 x$$

$$H = \frac{p^2}{2} + \varepsilon_0 x + \varepsilon x \cos\omega t$$

$$x > 0$$

(Benvenuto, Casati, Guarneri, D.S. (1991).

Oscillating frame → oscillating wall

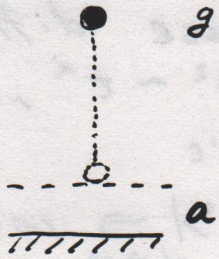

$$x_w = -\frac{\varepsilon}{\omega^2}\cos\omega t; \qquad a = \frac{\varepsilon}{\omega^2};$$

$$V_w = \frac{\varepsilon}{\omega}\sin\omega t$$

$$\bar{p} = p - 2V_w = p - \frac{2\varepsilon}{\omega}\sin\phi$$

$$\bar{\phi} = \phi + 2\cdot\omega\cdot\Delta t = \phi + 2\frac{\omega\bar{p}}{\varepsilon_0}$$

Chaos border $K = kT = 4\varepsilon/\varepsilon_0 > 1$

Map in canonical variables:

$$N = E/\omega = p^2/2\omega$$

$$\begin{cases} \bar{N} = N + \frac{2\varepsilon}{\omega^2}\sqrt{2\omega\bar{N}}\sin\phi \\ \bar{\phi} = \phi + \frac{2\omega}{\varepsilon_0}\sqrt{2\omega\bar{N}} + O(\varepsilon) \end{cases}$$

power law localization

$\varepsilon < \varepsilon_c$

$\psi_N \sim 1/N^2$

$\ell = \frac{\omega^3}{4\varepsilon^2}$

$$D = \frac{k^2}{2} = \frac{4\varepsilon^2}{\omega^3}N; \quad \rightarrow \ell_\phi = D = \frac{4\varepsilon^2}{\omega^3}N > N$$

Delocalization border: $\varepsilon > \varepsilon_c = \frac{1}{2}\omega^{3/2}$

Benvenuto, Casati, Guarneri, Shepelyansky (1991)

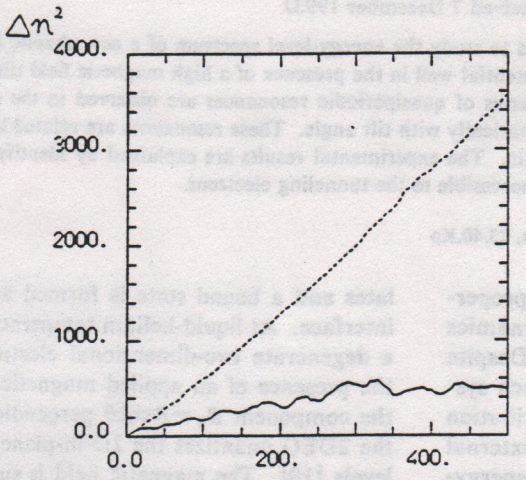

Fig. 1. The numerically computed 2nd moments Δn^2 of the distribution in the unperturbed action variable n. as a function of time (given in number $\bar{t}$ of periods of the perturbing field). for $\omega = 2.52$, $\varepsilon = 0.5$, $\varepsilon_0 = 0.4$, $n_0 = 60$. The classical motion (dashed line) is diffusive while the quantum (full line) saturates. Here is $\varepsilon_{cr}^{(Q)} \sim 2.0$

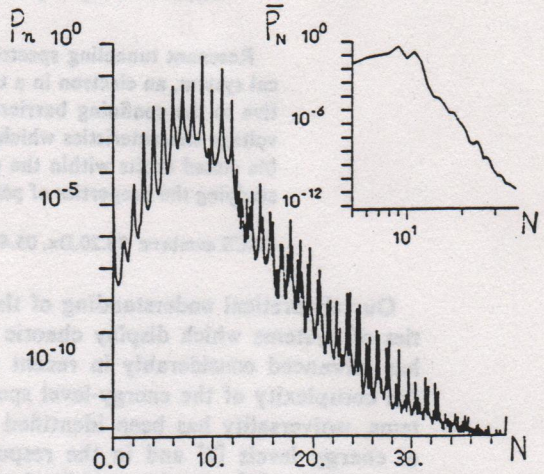

Fig. 3. a A localized distribution: the probability of occupation P_n of the unperturbed state n. versus N. in logarithmic scale. Here $\omega = 2.52$, $\varepsilon = 0.5$, $\varepsilon_0 = 0.4$, $n_0 = 60$. b The total probability $\overline{P_N}$ within the N-th photon zone, versus N in double logarithmic scale

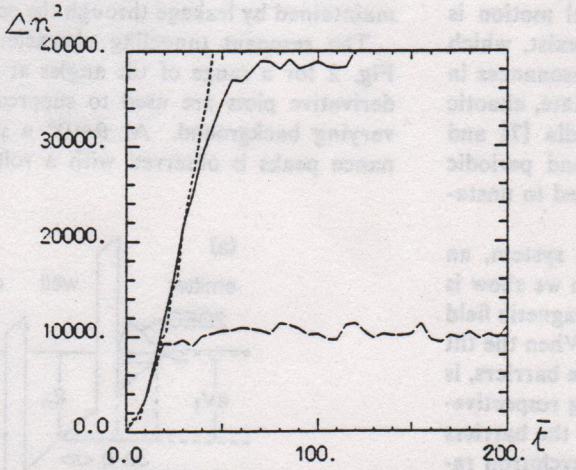

Fig. 2. Same as Fig. 1. with $\omega = 0.6$. Here $\varepsilon_{cr}^{(Q)} \sim 0.2324$. Two quantum curves are shown with basis size 384 (broken line) and 738 (full line)

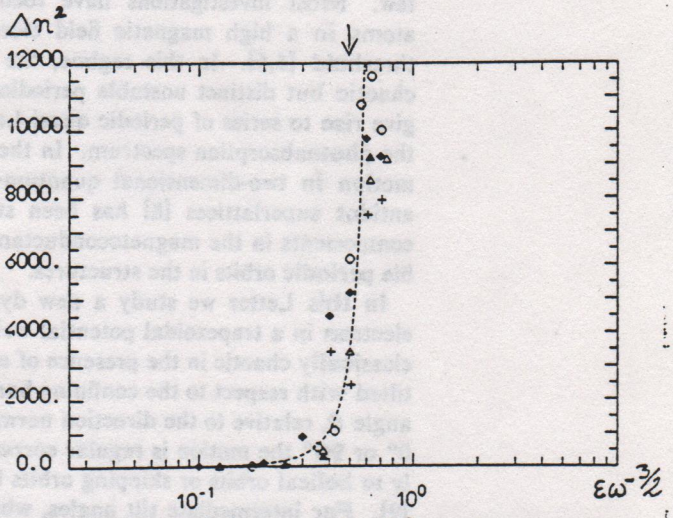

Fig. 4. The spread of the wave packet Δn^2 over the unperturbed states (2nd moment of the distribution in n), averaged in time from 100 to 200 field periods, versus the decimal logarithm of the variable $\varepsilon\omega^{-3/2}$ for $n_0 = 5$: Full diamonds: $\omega = 1.00$, $\varepsilon_0 = 0.2$; Circles: $\omega = 2.00$, $\varepsilon_0 = 1.0$; Triangles: $\omega = 2.52$, $\varepsilon_0 = 0.4$; Crosses: $\omega = 4.60$, $\varepsilon_0 = 1.44$ and for $n_0 = 10$: Full triangles: $\omega = 2.52$, $\varepsilon_0 = 0.4$. The dashed line is drawn to guide the eye

Fig. 1. enlarging the basis does not lead to any significant modification of the wave packet evolution.

Due to obvious computational limitations the basis could not be further enlarged. Strictly speaking, the obtained numerical data do not therefore answer the question. whether the observed transition is a real delocalization due to the appearance of a continuous spectral component, or just a localization on a much larger scale. On the other hand, a numerical computation can hardly be expected to yield better evidence than the clear crossover illustrated by our data.

The above results clearly show that the quantum dynamics of this model is quite different from that of the quantized standard map (5).

Figure 4 provides a check for the validity of the estimate (10) for the critical field for delocalization. The data in Fig. 4 illustrate how the localization (measured by the spread of the wavepacket after a fixed time) is destroyed upon increasing ε while keeping ω fixed. The data in Fig. 4 correspond to four different values of ω. In each case, the spread increases more or less sharply from 0 to a saturation value (which is determined by the filling up of the finite basis set). In Fig. 4 the spread is plotted (in semi-logarithmic scale) against the variable $\varepsilon\omega^{-3/2}$ that, according to (10,11) is the same as $\varepsilon/\varepsilon_{cr}^{(Q)}$.

Magnetotunneling Spectroscopy of a Quantum Well in the Regime of Classical Chaos

T. M. Fromhold, L. Eaves, F. W. Sheard, M. L. Leadbeater,* T. J. Foster, and P. C. Main

Department of Physics, University of Nottingham, Nottingham NG7 2RD, United Kingdom

(Received 7 December 1993)

Resonant tunneling spectroscopy is used to study the energy-level spectrum of a new chaotic dynamical system, an electron in a trapezoidal potential well in the presence of a high magnetic field tilted relative to the confining barriers. Distinct series of quasiperiodic resonances are observed in the current-voltage characteristics which change dramatically with tilt angle. These resonances are related to unstable closed orbits within the chaotic domain. The experimental results are explained by identifying and studying the properties of periodic orbits accessible to the tunneling electrons.

PACS numbers: 73.20.Dx, 05.45.+b, 73.40.Gk, 73.40.Kp

Our theoretical understanding of the quantum properties of systems which display chaotic classical dynamics has advanced considerably in recent years [1]. Despite the complexity of the energy-level spectrum of such systems, universality has been identified in the distribution of energy levels [2] and in the response to an external perturbation [3]. In the semiclassical limit the energy-level pattern and spatial eigenfunctions have been related to the occurrence of closed classical orbits within the chaotic sea [1,4]. However, the experimental studies of quantum phenomena in nonintegrable systems have been few. Most investigations have focused on hydrogenic atoms in a high magnetic field close to the ionization threshold [5,6]. In this regime, the classical motion is chaotic but distinct unstable periodic orbits exist, which give rise to series of periodic quasi-Landau resonances in the photoabsorption spectrum. In the solid state, chaotic motion in two-dimensional quantum-dot stadia [7] and antidot superlattices [8] has been studied and periodic components in the magnetoconductance related to unstable periodic orbits in the structures.

In this Letter we study a new dynamical system, an electron in a trapezoidal potential well, which we show is classically chaotic in the presence of a high magnetic field tilted with respect to the confining barriers. When the tilt angle θ, relative to the direction normal to the barriers, is 0° or 90° the motion is regular corresponding respectively to helical orbits or skipping orbits between the barriers [9]. For intermediate tilt angles, when the cyclotron radius is sufficiently small, the orbit segments between successive collisions with the barriers rapidly become uncorrelated giving rise to strongly chaotic motion. As shown in Fig. 1, unstable periodic orbits also occur in this chaotic dynamic sea, for particular values of the initial electron velocity.

We have investigated the quantized energy-level spectrum associated with this classically chaotic system by incorporating the potential well into a double-barrier semiconductor heterostructure as in Fig. 1. In our experiments the GaAs quantum well (QW) of width $w=120$ nm is enclosed between $Al_{0.4}Ga_{0.6}As$ tunnel barriers of width $b=5.6$ nm surrounded by weakly n-doped (2×10^{16} cm^{-3}) contact layers [9]. Under bias, charge accumulates and a bound state is formed at the emitter-barrier interface. At liquid-helium temperatures this gives rise to a degenerate two-dimensional electron gas (2DEG). In the presence of an applied magnetic field $\mathbf{B}=(B_x,0,B_z)$, the component $B_x=B\cos\theta$ perpendicular to the plane of the 2DEG quantizes the 2D in-plane motion into Landau levels [10]. The magnetic field is sufficiently large (11.4 T) that, except for θ close to 90°, only the lowest Landau level is occupied. Resonant tunneling occurs when the energy of this discrete emitter state coincides with the energy ϵ_n of a subband in the QW [11]. As the bias voltage V is varied the tunneling electrons thus scan the energy-level spectrum of the QW. Continuity of the current I is maintained by leakage through the collector barrier.

The resonant tunneling characteristics are shown in Fig. 2 for a range of tilt angles at $B=11.4$ T. Second-derivative plots are used to suppress the monotonically varying background. At $\theta=0°$ a single series of resonance peaks is observed with a voltage period $\Delta V\cong30$

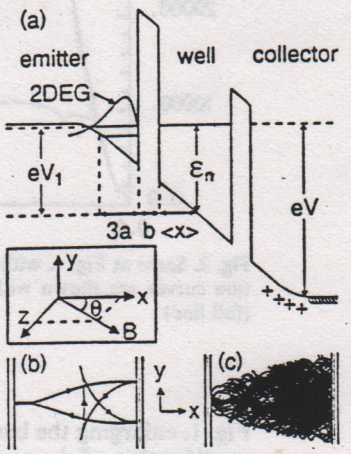

FIG. 1. (a) Conduction band profile of double-barrier structure under bias voltage V, showing resonant tunneling of electrons from emitter 2DEG into subband level ϵ_n in the well. Inset shows tilt angle θ of magnetic field B relative to tunneling (x) direction. (b) Projection in x-y plane of closed periodic orbit ($V=440$ mV, $B=11.4$ T, $\theta=20°$). (c) Chaotic orbit resulting from 0.1% change in initial electron velocity.

0031-9007/94/72(16)/2608(4)$06.00

Chaotic Landau levels mixing in classical and quantum wells

(D.S., D. Stone 1994)

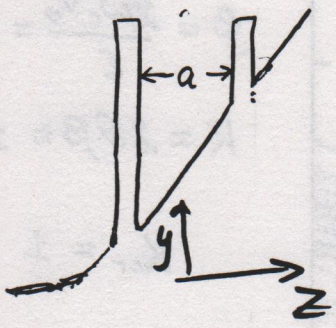

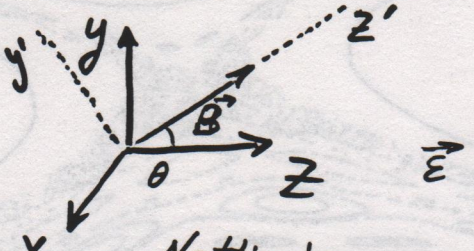

Nottingham Fromhold, Eaves et. al 1994

AT&T Müller, Boebinger, Mathur, Pfeiffer, West 1994

tilted magnetic field

chaotic trajectories

Chaos border for energy transfer between Landau levels and z-motion

$$\vec{A} = (-By\cos\theta + Bz\sin\theta,\ 0,\ 0) \qquad \text{(a.u.)}$$

$$H = \frac{(p_x - By\cos\theta + Bz\sin\theta)^2}{2m^*} + \frac{p_y^2}{2m^*} + \frac{p_z^2}{2m^*} + \mathcal{E}z$$

$p_x = \text{const} \longrightarrow$ 2-degrees of freedom $\omega_c = \frac{B}{m^*}$

Integrable motion between collisions

Map description: with wall (y', z'):

Kicked Top Haake 1986

$$\left.\begin{aligned} \bar{v}_{x'} &= v_{x'} \\ \bar{v}_{z'} &= \cos 2\theta\, v_{z'} - \sin 2\theta\, v_{y'} \\ \bar{v}_{y'} &= \sin 2\theta\, v_{z'} + \cos 2\theta\, v_{y'} \end{aligned}\right\} \bar{\bar{v}}_{z'} = \bar{v}_{z'} \rightarrow \text{collision}$$

$$\left.\begin{aligned} \bar{\bar{v}}_{y'} &= \cos\varphi\, \bar{v}_{y'} - \sin\varphi\, \bar{v}_{x'} \\ \bar{\bar{v}}_{x'} &= \sin\varphi\, \bar{v}_{x'} + \cos\varphi\, \bar{v}_{x'} \end{aligned}\right\} \text{Larmor rotation}$$

$$\varphi = \frac{2\omega_c \bar{v}_{z'}}{\mathcal{E}\cos\theta} \quad \text{1 wall}$$

$$\varphi = \omega_c a / \bar{v}_{z'}\cos\theta \quad 2 \text{ walls}$$

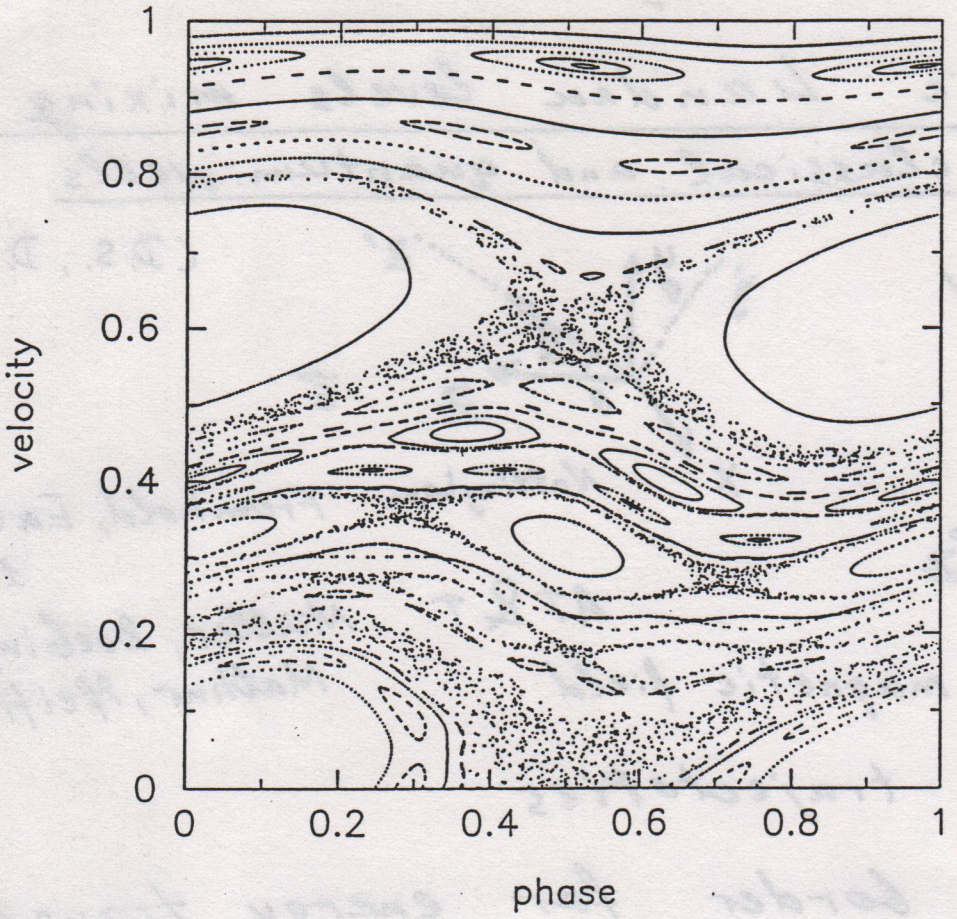

$\theta = 0.05$

$\beta = \frac{2\omega_c V_0}{\varepsilon} = 10$

$K \approx 2\theta\beta \approx 1$

$K_{cr} = 1$

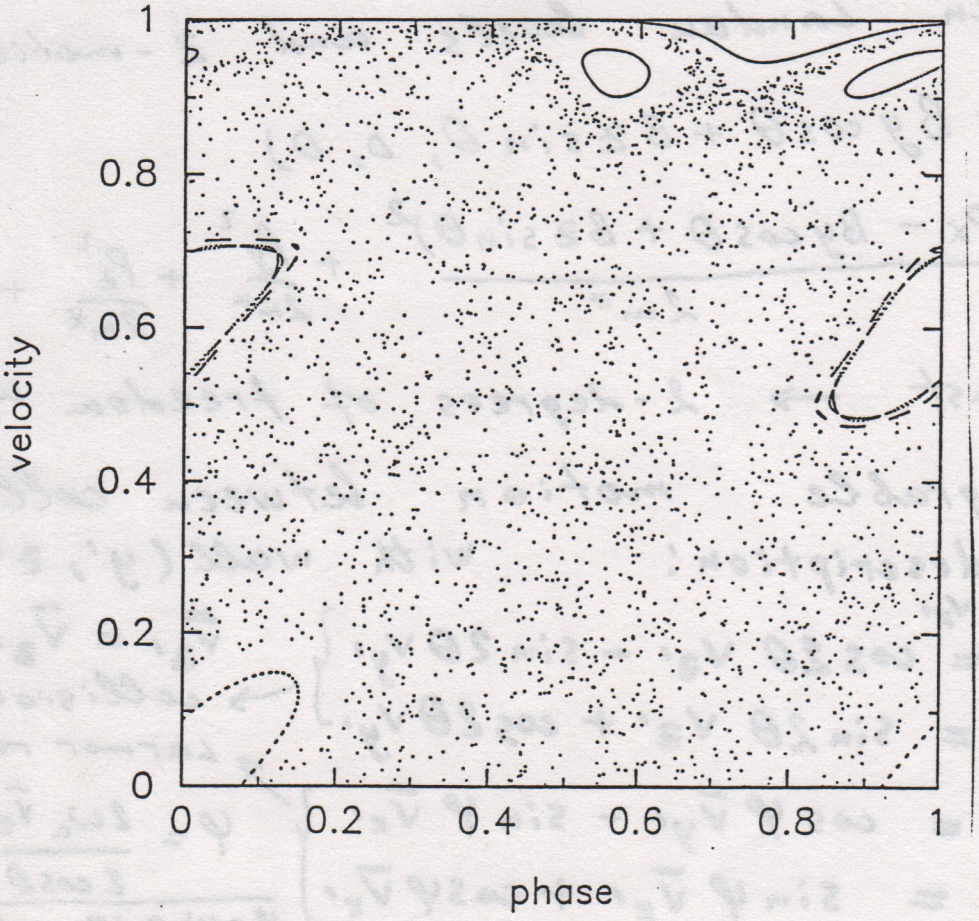

$\theta = 0.15$

$\beta = 10$

$K \approx 3$

Map for small angels : Chirikov standard map

$$\bar{v}_z = v_z - v_0 \sin 2\theta \sin\phi \qquad T = \frac{2\omega_c v_0}{\varepsilon}$$

$$\bar{\phi} = \phi + \frac{2\omega_c \bar{v}_z}{\varepsilon \cos\theta} \qquad k = \sin^2\theta$$

$$K = kT = 2\sin\theta \cdot \frac{2\omega_c v_0}{\varepsilon} > 1 \quad \text{chaos border}$$

In experiment $v_0 \approx \sqrt{2\varepsilon a \cos\theta / m^*}$

$$\omega_c^2 = \frac{B^2}{m^{*2}} > \frac{\Delta V}{32\theta^2 a^2 m^*}$$

$B = 12\ T$
$m^* = 0.067$
$\theta = 27^\circ$
$\Delta V_{cr} \approx 0.15\ V$

Quantum localization (as in triangular well); $N_0 = E_{tot}/\omega_c$

$$\bar{N} = N - 4\theta\sqrt{N_0 \bar{N}}\sin\phi$$

$$\bar{\phi} = \phi + \frac{2\omega_c}{\varepsilon}\sqrt{2\omega_c \bar{N}} + O(\theta)$$

$$l = D = 8\theta^2 N_0 N > N$$

Ergodic eigenstates for

$$8\theta^2 N_0 > 1$$

In experiment $V = 1eV$, $B = 10\ T \rightarrow N_0 \approx 60$

$\theta > 3^\circ$

Two walls without electric field

collision

$$\bar{V}_{z'} = -\cos 2\theta\, V_{z'} + \sin 2\theta\, V_{y'}$$
$$\bar{V}_{y'} = \sin 2\theta\, V_{z'} + \cos 2\theta\, V_{y'}$$
$$\bar{V}_{x'} = V_{x'}$$

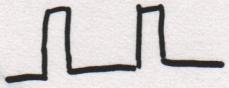

Larmor rotation

$$\bar{\bar{V}}_{y'} = \cos\varphi\, \bar{V}_{y'} - \sin\varphi\, \bar{V}_{x'}$$
$$\bar{\bar{V}}_{x'} = \sin\varphi\, \bar{V}_{x'} + \cos\varphi\, \bar{V}_{x'}$$
$$\bar{\bar{V}}_{z'} = V_{z'}$$

$$\varphi = \frac{\omega_c d}{|\bar{V}_{z'}|\cos\theta}$$

For small θ: Fermi arcelaration mode.

$$\bar{V}_{z'} \simeq -V_{z'} + 2\theta\, V_0 \cos\phi$$
$$\bar{\phi} = \phi + \frac{\omega_c d}{|\bar{V}_{z'}|}$$

Chaos border

$$K = \frac{2\theta\, \omega_c d\, V_0}{V_z^2} > 1$$

Higher dimensions

$$H = H_0(n) + V(\theta, \omega_1 t, \omega_2 t)\, \delta_1(t)$$

Extended phase-space

$$\theta_1 = \omega_1 t \; ; \quad \theta_2 = \omega_2 t$$

$$\tilde{H} = \underbrace{H_0(n) + \omega_1 n_1 + \omega_2 n_2}_{\to \tilde{H}_0(n, n_1, n_2)} + V(\theta, \theta_1, \theta_2)\, \delta_1(t)$$

exact transformation due to linearity in n_1, n_2

$$\bar{\Psi} = U \Psi \; ; \quad U = e^{-i \tilde{H}_0(n, n_1, n_2)} \; e^{-i V(\theta, \theta_1, \theta_2)}$$

Equivalent to 3D solid-state lattice for ω_1, ω_2

2D for ω_1 ; $(\omega_2 = 0)$

$\omega_1 \to \ln l \sim D$ (D.S. 1983)

$\omega_1, \omega_2 \to$ Anderson transition $V > V_{cr}$

↑ gain of numerical factor N^2

(Casati, Guarneri, D.S. (1989))

$$V = -2 \tan^{-1}\left[2k(\cos\theta + \cos\theta_1 + \cos\theta_2)\right]$$

$$\gamma = 3.5\, |k - 0.4691|^{1.5}$$

$$D = 2.51\, |k - 0.4651|^{1.25}$$

with conjugates momenta n_1 and n_2. Then we consider the Hamiltonian

$$H' = H_0(\hat{n}) + \omega_1\hat{n}_1 + \omega_2\hat{n}_2 + V(\theta,\theta_1,\theta_2)\sum_{s=-\infty}^{+\infty}\delta(t-s)\,, \quad (5)$$

with $\hat{n}_{1,2} = -i\,\partial/\partial\theta_{1,2}$. Equation (5) describes a quantum rotator with three freedoms $(\theta,\theta_1,\theta_2)$ subjected to periodic kicks, the strength of which is not explicitly time dependent. The one-period propagator for this rotator is the unitary operator

$$e^{-iV(\theta,\theta_1,\theta_2)}e^{-i[H_0(\hat{n})+\omega_1\hat{n}_1+\omega_2\hat{n}_2]}\,.$$

In order to show that the 3D quantum model defined by (5) and the 1D model defined by (1) and (3) are substantially equivalent, we rewrite the Schrödinger equation for the 3D model

$$i\,d/dt\,\psi(\theta,\theta_1,\theta_2,t) = H'\psi(\theta,\theta_1,\theta_2,t)\,,$$

in the interaction representation defined by

$$\psi(\theta,\theta_1,\theta_2,t) = e^{-i(\omega_1\hat{n}_1+\omega_2\hat{n}_2)t}\bar{\psi}(\theta,\theta_1,\theta_2,t)\,. \quad (5a)$$

In this way we obtain

$$i\,d\bar{\psi}/dt = H_0\bar{\psi} + V(\theta,\theta_1+\omega_1 t,\theta_2+\omega_2 t)\sum_{s=-\infty}^{+\infty}\theta(t-s)\bar{\psi}\,,$$

i.e., the Schrödinger equation for the evolution of the 1D model.

We can now apply a transformation to the three rotator (5), which was originally devised in Ref. 2 for the standard, 1D kicked rotator and was subsequently generalized in Ref. 11. Because of this transformation the problem of our determining the quasienergy eigenvalues and eigenvectors for the three rotator turns out to be formally equivalent to solving the equation

$$T_{\mathbf{n}}u_{\mathbf{n}} + \sum_{\mathbf{r}\neq 0} W_{\mathbf{r}}u_{\mathbf{n}+\mathbf{r}} = \epsilon u_{\mathbf{n}}\,, \quad (6)$$

where $\mathbf{n}\equiv(n,n_1,n_2)$ and $\mathbf{r}$ label sites in a 3D lattice,

$$T_{\mathbf{n}} = -\tan[\tfrac{1}{2}(E_n + n_1\omega_1 + n_2\omega_2 + \lambda)]\,,$$

λ is quasienergy, $W_{\mathbf{r}}$ are coefficients of a threefold Fourier expansion of $\tan[\frac{1}{2}V(\theta,\theta_1,\theta_2)]$, and $\epsilon = -W_0$.

We now choose

$$V(\theta,\theta_1,\theta_2) = -2\tan^{-1}[2k(\cos\theta+\cos\theta_1+\cos\theta_2)]\,, \quad (6a)$$

so that (6) becomes

$$T_{\mathbf{n}}u_{\mathbf{n}} + k\sum_{\mathbf{r}}{}'u_{\mathbf{r}} = 0\,, \quad (7)$$

where the sum $\sum'$ includes only the nearest neighbors to $\mathbf{n}$. The tight-binding model (7) with the potential $T_{\mathbf{n}}$ is in a sense equivalent to the original rotator problem. The quasienergy eigenfunctions of the rotator will be localized or extended over the unperturbed eigenstates of H_0, depending on whether the tight-binding model has localized or extended eigenstates; in the localized case, the localization length will be the same. Since the dynamics of the rotator is determined by the nature of its quasienergy eigenstates, any change from localized to extented states that may take place in the tight-binding model (7), as the coupling parameter k is increased, will be mirrored by a simultaneous change in the rotator dynamics, from a localized recurrent behavior to an unending spreading over the unperturbed base. As we mentioned above, the latter type of transition can be numerically detected with less effort than by our directly tackling the tight-binding model.

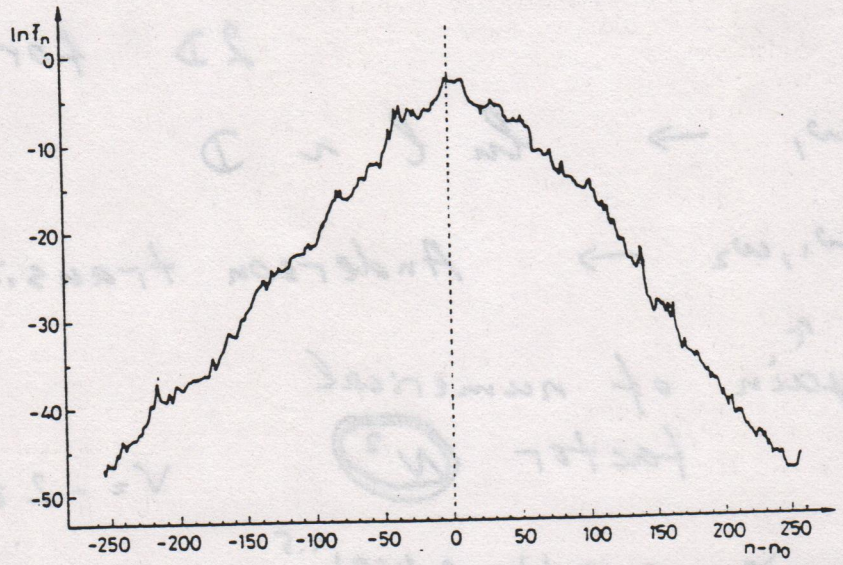

FIG. 1. Example of localized steady-state probability distribution $\bar{f}_n$ over the unperturbed levels averaged over 5000 iterations within the interval $95000 < t < 100000$. Here parameter $k = 0.38$.

134

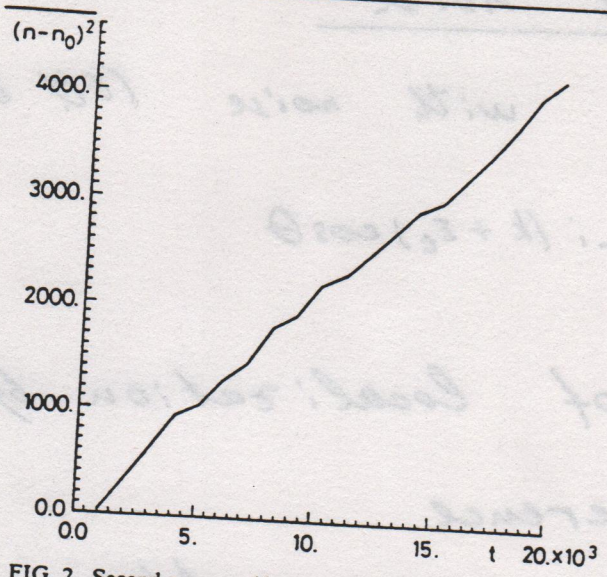

FIG. 2. Second moment $\langle (n-n_0)^2 \rangle$ of the probability distribution as a function of time t (in number of iterations) in the delocalized regime. Here parameter $k=0.6$.

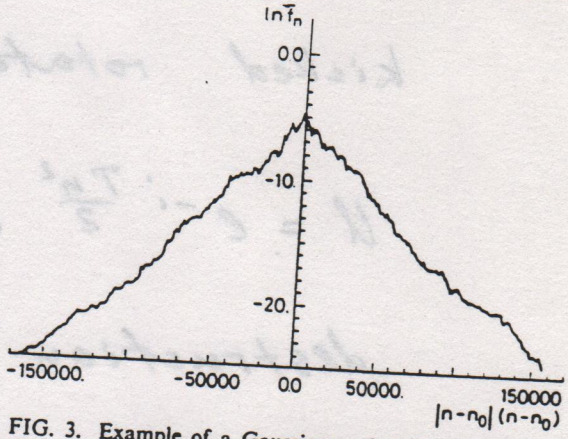

FIG. 3. Example of a Gaussian probability distribution $\bar{f}_n$ over the unperturbed levels for the same case of Fig. 2. The probability distribution is here averaged over 1000 iterations within the interval $19000 < t < 20000$.

The disorder in the model (7) is given by the pseudorandom character of the potential T_m. We remark that by replacing $n_1\omega_1$ and $n_2\omega_2$ by random numbers, one would get a 3D Lloyd model. In that case, however, the time dependence of V could not be made explicit as in Eq. (4). One should then numerically simulate a 3D rotator rather than a 1D one, with a consequent sharp reduction of the allowable number of iterations.

The model was investigated by numerical simulation of the quantum dynamics defined by (1) with phases $\theta_1=\theta_2=0$. A basis of unperturbed eigenstates up to 512 was used. The initial state was chosen in the middle of this base and its time evolution was numerically determined by iteration of the quantum map (4) giving the one-period evolution, up to 10^5 iterations, for different values of the perturbation parameter k. A transition between two different types of motion was observed around a value $k_{cr}\sim 0.47$, with localization occurring for $k<k_{cr}$ and unbounded diffusion taking place for $k>k_{cr}$. In the localized regime, the time-averaged steady-state distributions were found to decay exponentially with the level number (Fig. 1), so that the corresponding average localization lengths could be determined by our fitting the probability distributions with the exponential law $\exp(-2|n-n_0|/l)$. In the delocalized regime, unbounded diffusive excitation occurs and the related diffusion rates were determined by two ways; first, from the time dependence of the second moment of the probability distributions (Fig. 2), and, second, by our fitting the probability distributions with the Gaussian form which would be predicted by the diffusion law (Fig. 3).

By this second fitting we also obtained the number of levels which were effectively involved in the diffusion. In all cases, these levels were found to be a fraction close to 1 of the total number of levels, i.e., practically all states were delocalized. This was further confirmed by the closeness of the values of the diffusion coefficients obtained according to the two above described methods.

In Fig. 4 we show the dependence of the diffusion rate $D=\langle (n-n_0)^2 \rangle/t$ (in the delocalized regime) and of the inverse localization length $\gamma=l^{-1}$ (in the localized regime) on the perturbation parameter k. In order to suppress fluctuations, for each fixed value of k the values of γ and D were computed for ten different realizations of the random spectrum of H_0, and average values were

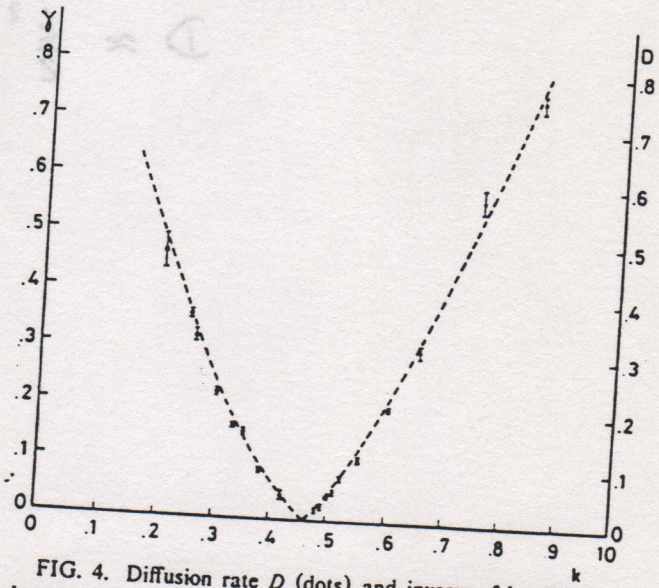

FIG. 4. Diffusion rate D (dots) and inverse of localization length $\gamma=1/l$ (circles) as a function of perturbation parameter k. Error bars were obtained from statistics over ten different realizations of the random spectrum. The dotted lines result from a three parameters least-squares fit (MINUIT) of numerical data.

(59)

Effects of noise

kicked rotator with noise (Ott et.al. (1984))

$$U = e^{-i\frac{Tn^2}{2}} e^{-i(k+\varepsilon_t)\cos\theta}$$

destruction of localization by noise:

time of coherence

$$(\Delta n)^2 \sim \varepsilon^2 t_c \sim 1 \longrightarrow t_c \sim 1/\varepsilon^2 \gg t^* \sim k^2$$

$$D_{noise} \sim \frac{l^2}{t_c} \sim$$ (jump on one l during time t_c)

$$\sim \varepsilon^2 l^2 \sim k^4 \varepsilon^2 \gg \varepsilon^2$$

$$D \approx \frac{k^2}{2} \gg D_{noise} \gg \varepsilon^2$$

$(k\varepsilon \ll 1, k \gg 1)$

(60)

Adiabatic destruction of Anderson localization

(Borgonovi, D.S. (1994))

Slow parameter variation with typical frequency $\omega \to 0$

$$i\dot{\psi}_n = E_n \psi_n + V(1+\varepsilon(t))(\psi_{n+1} + \psi_{n-1}); -W \le E_n \le W$$

$$\varepsilon(t) = \varepsilon(\sin(\omega_1 t) + \sin(\omega t)); \quad \varepsilon \sim 0.5$$

$\omega_1/\omega = 1.618\ldots$ golden mean

$\omega \to 0$ $\qquad l \approx 25\left(\frac{V}{W}\right)^2$

$D(\omega) \sim \omega^{\alpha}$ adiabatic noise

$\alpha = 0.74 \pm 0.02$ numerical result

$\alpha = 2/3$ theoretical value

Theory is based on Mott picture of energy absorbtion:

$D_E = (\Delta E)^2/t$; $\quad \Delta p \sim \Delta E/V \sim (D_E t)^{1/2}/V$

$E = 2V\cos p$;

spreading in space:

$$\Delta x \sim \Delta n \sim V \Delta p\, t \sim \sqrt{D_E}\, t^{3/2} \sim l \to t_c$$

$$t_c \sim \left(\frac{l^2}{D_E}\right)^{1/3} \longrightarrow D \approx \frac{l^2}{t_c} \sim l(l D_E)^{1/3}$$

(61) Rate of energy absorbtion:

$$D_E \sim \omega^2 \Gamma ; \quad \Gamma \sim F^2 \rho ; \quad \rho \sim 1/V$$

$$F \sim \varepsilon V \rightarrow$$

$$\frac{D}{\ell} \sim (\varepsilon \omega \ell \sqrt{V})^{2/3}$$

Kicked rotator with modulated kick amplitude

$$U = \exp(-i \frac{T n^2}{2}) \exp(-i k(t) \cos\theta)$$

$$k(t) = k(1 + \varepsilon_1 \cos\omega t + \sin\omega_1 t))$$

$$\alpha = 0.73 \pm 0.02$$

Electrons in 1d random potential and slow-varying electric field

$$F \sim \sum_{n'} |\mathcal{E}(t) \times |n'\rangle \sim \mathcal{E} \ell \ln(V/\omega)$$

$$D \sim \left[\frac{\omega^2 \mathcal{E}^2 \ell^7 \ln^2(V/\omega)}{V} \right]^{1/3}$$

[8] B.Kramer and A.MacKinnon, Rep. Prog. Phys., 56, 1469 (1993).
[9] S.Fishman and D.L.Shepelyansky, Europhys. Lett. 16, 643 (1991).
[10] D. Cohen, Phys. Rev. A, 44, 2292 (1991).
[11] E.Ott, T.M.Antonsen Jr, and J.D.Hanson Phys. Rev. Lett. 53, 2187 (1984).
[12] This value of ϵ can not be considered small enough to use the ϵ-dependence estimate given by (3). In fact one should also take into account that both V and l should be replaced by the approximate ϵ-dependent expressions $V \to V(1+2\epsilon)$ and $l \to l(1+2\epsilon)^2$. This gives $D \propto (1+2\epsilon)^{11/3}\epsilon^{2/3}$. Our numerical data for variation of ϵ in the interval [0.25, 0.8] are in agreement with such correction. To have $D \propto \epsilon^{2/3}$ the value of ϵ should be sufficiently small. This however requires large l that makes numerics quite heavy.
[13] F. Izrailev, Phys. Rep. 196, 299 (1990).
[14] Note that the matrix elements between double-hump states are $\langle m|\cos\theta|m'\rangle \sim 1$, while their typical values between localized states are $l^{-1/2}$ [4].
[15] R.Blumel, U.Smilansky, Phys. Rev. Lett. 69, 217 (1992).
[16] B.V.Chirikov, CERN Trans. 71-40, Geneva (1971); A.B.Rechester, M.N.Rosenbluth and R.B.White, Phys. Rev. Lett. 42, 1247 (1979).
[17] G.Paladin and A.Vulpiani, J. Phys. A, 19, 1881 (1986); G.Parisi and A.Vulpiani, J. Phys. A 19, L425 (1986).

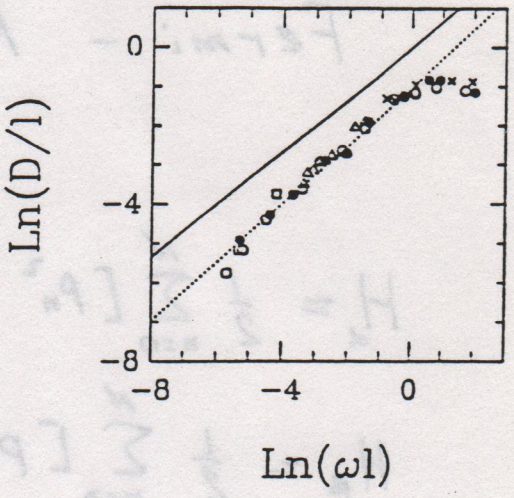

FIG. 2. Diffusion rate D as a function of the rescaled variables for the model (1) with $V = 1$, $\epsilon = 0.5$, $l = 25(V/W)^2$, $\omega_1/\omega = 1.618...$ $E = 0$. Symbols are: o for $W = 1.5$, • for $W = 1$, × for $\omega = 0.07$, △ for $\omega = 0.005$, and □ for $\omega = 0.0003$. Dashed line represents the least squares fit while the full line shows the theoretical slope $\alpha = 2/3$.

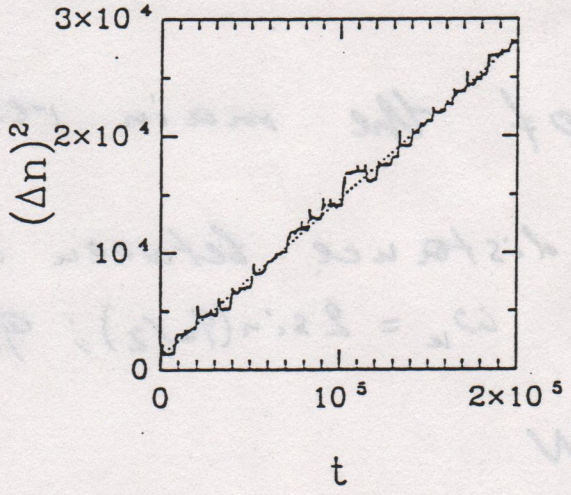

FIG. 1. Dependence of the square width of wave packet as a function of time for the model (1), with $W = 1.5$, $\omega = 0.001$, $\omega_1/\omega = 1.618...$, $V = 1$, $\epsilon = 0.5$. The size of the lattice is $N = 2048$. Initially, only one site level is excited with energy $E = 0$. The dashed line shows the linear fit with $D = 0.135$.

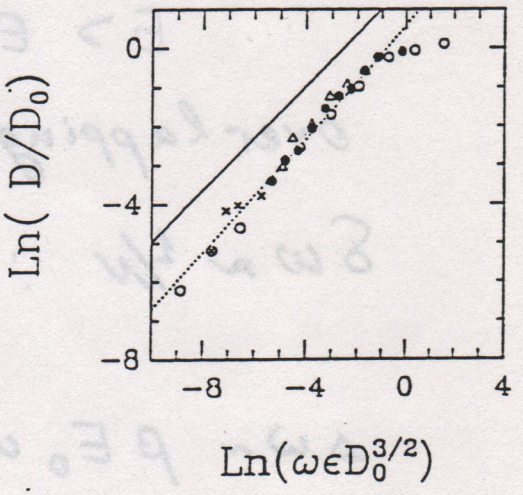

FIG. 3. Diffusion rate D as a function of the rescaled variables for the model (1) with $kT = 6$, $\omega_1/\omega = 1.618...$, $D_0 = k^2/2$. Symbols are: o for $k = 3$, $\epsilon = 0.5$; • for $\omega = 0.001$, $\epsilon = 0.5$; × for $\omega = 0.0001$, $\epsilon = 0.5$; △ for $\omega = 0.001$, $k = 10.08$. Dashed line represents the least squares fit while the full line shows the theoretical slope $\alpha = 2/3$.

Borgonovi, D.S. (1994)

139

Fermi - Pasta - Ulam problem (1955)

$$H_\alpha = \frac{1}{2}\sum_{n=0}^{N}\left[p_n^2 + (x_{n+1}-x_n)^2\right] + \frac{\alpha}{3}\sum_{n=0}^{N}(x_{n+1}-x_n)^3$$

$$H_\beta = \frac{1}{2}\sum_{n=0}^{N}\left[p_n^2 + (x_{n+1}-x_n)^2\right] + \frac{\beta}{4}\sum_{n=0}^{N}(x_{n+1}-x_n)^4$$

Estimate for chaos border in β-model (Chirikov, Izrailev (1966). (1973)

$E > E_{cr}$

over-lapping of the main resonances

$\delta\omega \approx 1/N$: - distance between resonances

$$\omega_k = 2\sin(q_k/2);\quad q_k = \frac{\pi k}{N+1}$$

$\Delta\omega \sim \beta E_0 \omega_k / N$

$\rightarrow \beta E_0 > N/k \sim 1/\omega_k$

Reward to those
who passed through the
course:

If you studied well the problems
Of nonlinear equations
You can go to Las Vegas
And to beat Roulette
(instead of) for thesis
As it was done
By Farmer Doyne

1) Problem S1

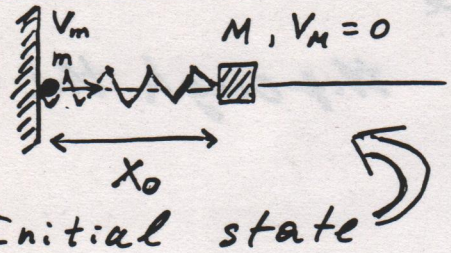

Initial state

spring $F_M = -kx$

$M \gg m$

To find: equilibrium position, effective potential and frequency of small oscillations for heavy mass M.

---

2) PS2 Two-colors dynamics of homogeneous classical Yang-Mills fields with mass is described by effective Hamiltonian:

$$H = \frac{1}{2}(E_1^2 + E_2^2 + A_1^2 + A_2^2 + A_1^2 A_2^2)$$

(E_i, A_i - are canonically conjugated variables as momentum and coordinat

In the limit of small energy $E \to 0$ (small nonlinearity):

to find: phase-space picture of motion, frequency of small oscillations near equilibrium, allowed energy exchange between modes.

Instruction: keep resonant terms in the Hamiltonian

PS1

Problem S3

In one-dimensional model of classical helium atom to find stable configurations in which both electrons are located from one side of the charged center (see fig. S3). Find effective potential for outside electron, equilibrium position and frequency of small oscillations. Analyse the case of different center charge Z. Compare analytical results with numerical simulations of

K. Richter, D. Wintgen et. al. (a) PRL 65 (1990) 1965;
(b) J. Phys. B: At. Mol. Opt. Phys. 25 (1992) 3929;
(c) PRA 48 (1993) 4182

Instruction!

to assume that the inner electron (e_1) moves over 1D Kepler orbit with high frequency.

Use atomic units.

$\frac{x_{min}}{2a} = ?$

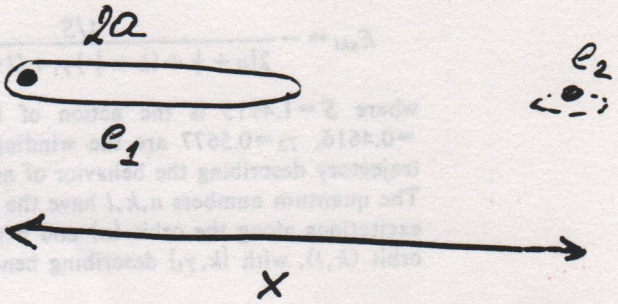

Fig. S3

(see also Fig. in ref. a)

Possible extention to 2D case ?

Stable Planetary Atom Configurations

A proper description of highly doubly excited atoms or ions is still an outstanding problem of "elementary" quantum mechanics. Current interest both experimentally and theoretically is focused on highly correlated electron motion, where any independent-particle model is inadequate to describe the properties of such states.

In a recent publication[1] Eichmann, Lange, and Sandner reported on the observation of planetary atomic states, where two electrons of a barium atom were both in highly excited states. The authors could reproduce their data quite well within a "frozen-planet approximation" (FPA), where one electron is fixed at some radial distance, whereas the other electron moves in the field of the residual barium ion and of the frozen electron. The remarkable success of their model indicates that there is a dynamical mechanism behind the *ad hoc* assumption of a frozen electron at large radial distances. We will comment on this mechanism and show that indeed there are classically stable configurations, which are close to the frozen-planet configuration of Ref. 1.

Our procedure to solve the classical equations of motion for the general three-body Coulomb problem are described elsewhere.[2] Here we focus on the helium atom with total angular momentum $J=0$. Because of inherent classical scaling properties the results are valid for all (negative) energies.[2] Most of the classical orbits are unstable and ionize, but stable bound motion does also exist. The most stable configuration we found is a collinear one, where both electrons are on the same side of the atom and where both electrons oscillate with the same frequency. The radial extents of these motions are very different and are indicated in Fig. 1(a). The stability of the motion is rather insensitive to variations in initial conditions. This is exemplified in Fig. 1(b), which shows the (regular) motion for slightly different initial conditions. It is obvious from Fig. 1(a) that the *dynamical* configuration of the electrons is very close to the FPA configuration considered in Ref. 1, which explains the success of their model.

It is straightforward to quantize the motion semiclassically.[3] Associated with the regular phase-space volume around the dynamical FPA orbit is a series of resonances converging to the double-ionization threshold. The resonance energies are given by (atomic units)

$$E_{nkl} = -\frac{1/S}{2[n+\frac{1}{2}+(k+\frac{1}{2})\gamma_1+(l+\frac{1}{2})\gamma_2)]^2}, \quad (1)$$

where $S=1.4915$ is the action of the orbit and $\gamma_1=0.4616$, $\gamma_2=0.5677$ are the winding numbers of the trajectory describing the behavior of nearby trajectories. The quantum numbers n,k,l have the meaning of nodal excitations along the orbit (n) and perpendicular to the orbit (k,l), with $\{k,\gamma_1\}$ describing bending motion. n is unlimited, but the upper limits of k,l depend on n. Semiclassically these states are bound, but they can decay quantum mechanically by (dynamical) tunneling. The decay times T for such processes are typically exponentially small, that is $\ln(T)\approx -n$, with n defined above.

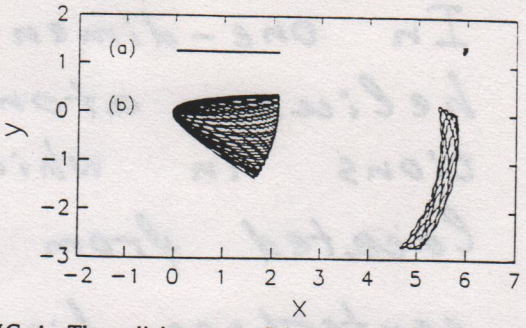

FIG. 1. The radial extents of the electrons for (a) the FPA periodic orbit, and (b) a nonperiodic but regular trajectory in its neighborhood.

The charge distributions of the associated wave functions show a huge gap between the turning point of the inner electron and the localization of the frozen electron. Therefore, laser excitation of such states *must* occur in multiple steps, as has been done in Ref. 1. The states should also show up in experiments using coherent laser excitation of wave packets.[4] In such an experiment the first laser pulse prepares the outer wave packet and a second laser pulse excites the inner one. The time delay between the two laser pulses plays a crucial role: The outer wave packet has to be at its turning point when the second wave packet is excited.

This work was supported by the Deutsche Forschungsgemeinschaft under Contract No. Wi 877/2. We are grateful to J. S. Briggs for various discussions.

K. Richter[(1)] and D. Wintgen[(2)]
[(1)]Fakultät für Physik
Universität Freiburg
Hermann-Herder-Strasse 3
7800 Freiburg, West Germany
[(2)]Max-Planck-Institut für Kernphysik
Postfach 103 980
6900 Heidelberg, West Germany

Received 30 July 1990
PACS numbers: 31.50.+w, 32.30.Jc, 32.80.Dz, 32.80.Rm

[1]U. Eichmann, V. Lange, and W. Sandner, Phys. Rev. Lett. **64**, 274 (1990).
[2]K. Richter and D. Wintgen, J. Phys. B **23**, L197 (1990).
[3]M. C. Gutzwiller, J. Math. Phys. **12**, 343 (1971); W. M. Miller, J. Chem. Phys. **63**, 996 (1975).
[4]J. A. Yeazell, M. Mallalieu, and C. R. Stroud, Phys. Rev. Lett. **64**, 2007 (1990).

(144)

Problem S4

Wisker map describes the motion in chaotic layer near separatrix:

$$\bar{y} = y + \sin x$$

$$\bar{x} = x - \lambda \ln|\bar{y}|$$

To find the size of chaotic region in y for $\lambda \gg 1$.

Problem S5

For the Hamiltonian

$$H = \frac{I^2}{2} + k\cos(\theta + \lambda \sin \omega t)$$

to find the chaos border, and the size of chaotic modulational layer in I, $\lambda \gg 1$.

Instruction

Use asymptotic formula for Bessel function $J_n(\lambda)$.

(See recent experiment on this system by Mark Raizen PRL 73 (1994) 2974).

6) Problem S6.

Ping-Pong ball on oscillating wall in gravitational field (see Fig. S6). The wall oscillates according to the law: $x_w = a\cos\omega t$.

To find conditions under which the energy of ball E_6 grows to infinity and to determine how it grows with time $E_6(t)$. Reflection is elastic.

Instruction

derive canonical map for jumps of the ball of size $h \gg a$, to cosider 1D motion.

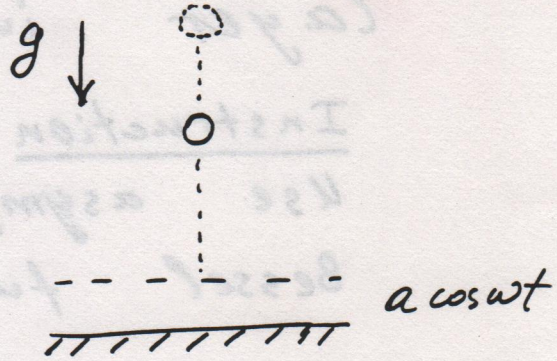

Fig. S6

PS4